



Cloud properties  
from satellite and  
ground

D. Merk et al.

This discussion paper is/has been under review for the journal Atmospheric Chemistry and Physics (ACP). Please refer to the corresponding final paper in ACP if available.

# Investigation of the adiabatic assumption for estimating cloud micro- and macrophysical properties from satellite and ground

D. Merk<sup>1</sup>, H. Deneke<sup>1</sup>, B. Pospichal<sup>2</sup>, and P. Seifert<sup>1</sup>

<sup>1</sup>Leibniz Institute for Tropospheric Research, Leipzig, Germany

<sup>2</sup>Leipzig Institute for Meteorology, Leipzig, Germany

Received: 26 January 2015 – Accepted: 5 February 2015 – Published: 24 February 2015

Correspondence to: D. Merk (merk@tropos.de)

Published by Copernicus Publications on behalf of the European Geosciences Union.

Title Page

Abstract

Introduction

Conclusions

References

Tables

Figures



Back

Close

Full Screen / Esc

Printer-friendly Version

Interactive Discussion



## Abstract

In this study we investigate the accuracy of quantities relevant for the first indirect aerosol effect, with focus on the cloud droplet number concentration and cloud geometrical depth. The adiabatic cloud model is commonly applied to retrieve cloud micro- and macrophysical quantities from passive satellite sensors like SEVIRI or MODIS. As reference we use ground-based observations from a cloud radar, a microwave radiometer and a ceilometer. The cloud geometrical depth is obtained directly from these measurements. An optimal estimation technique was developed to retrieve profiles of droplet number concentration. Although the ground-based observations contain detailed information about the cloud vertical structure, there are also large uncertainties. We investigate four different cases of temporally homogeneous and inhomogeneous liquid cloud layers. Considering uncertainties for both ground-based and satellite-based retrievals we found a good agreement for observations under suitable conditions. Overall cloud layers were subadiabatic with values of the subadiabatic factor consistent with previous studies. The best match between satellite and ground perspective is found for one of the homogeneous cases where we obtained a relative mean difference of adiabatic cloud geometrical depth of 15 % and a relative mean difference of cloud droplet number concentration of 27 %. The estimation of cloud droplet number concentration is especially sensitive to radar reflectivity for the ground-based retrieval and to effective radius for the satellite retrieval.

## 1 Introduction

Low-level liquid clouds play an important role in the energy balance of the earth, and are found in many areas around the globe. Their microphysical and optical properties are strongly influenced by aerosol particles that act as cloud condensation nuclei (CCN). Twomey (1974) first postulated the effect of an increased aerosol number concentration in clouds as a climatically relevant process. The quantification of such

ACPD

15, 5129–5173, 2015

### Cloud properties from satellite and ground

D. Merk et al.

Title Page

Abstract

Introduction

Conclusions

References

Tables

Figures



Back

Close

Full Screen / Esc

Printer-friendly Version

Interactive Discussion



aerosol indirect effects remains one of the main uncertainties in climate projections (Boucher et al., 2013).

If the liquid water content as well as the geometrical depth of the cloud are considered constant, a higher aerosol load directly results in an enhanced cloud albedo.

This effect is observed in particular by means of ship tracks that form in marine stratocumulus cloud decks (e.g. Ackerman et al., 2000). The chain of interactions of cloud microphysics and dynamics is complex and not yet fully understood. However, to quantify the effect of a change in the aerosol load on cloud albedo, it is necessary to consider both microphysics and macrophysics, which are influenced by cloud dynamical processes. Brenguier et al. (2000) noted that a 15% change in the cloud geometrical depth ( $H_{\text{cloud}}$ ) can have a similar effect on cloud albedo as a doubling of the cloud droplet number concentration ( $N_d$ ). Already Han et al. (1998) suggested to investigate a column cloud droplet number concentration which combines  $H_{\text{cloud}}$  and  $N_d$ . These two quantities turn out to be the key parameters for quantifying the aerosol effect on cloud albedo.

While both in-situ and remote sensing observations from ground do not cover large areas with high spatial resolution, passive satellite observations, although costly, show a good spatio-temporal coverage. Active satellite sensors such as the cloud profiling radar onboard CloudSat (Stephens et al., 2002) or the Cloud-Aerosol-Lidar with Orthogonal Polarization (CALIOP) onboard CALIPSO (Winker et al., 2009) are able to provide vertically resolved cloud observations over larger areas, but lack highly-resolved temporal coverage and have a smaller scanning swath than passive sensors onboard polar-orbiting satellites. For geostationary satellites, the high temporal resolution of up to 5 min is a big advantage, despite the reduced spatial resolution.

This motivated the evaluation of cloud parameters such as liquid water path ( $Q_L$ ) as in Roebeling et al. (2008b, a); Hünerbein et al. (2014) and  $H_{\text{cloud}}$  as in Roebeling et al. (2008a) obtained from SEVIRI with ground-based observations. To retrieve micro- and macrophysical properties of homogeneous liquid clouds from passive satellite instruments, commonly the adiabatic model is applied (e.g. Schueller et al., 2003; Boers

## Cloud properties from satellite and ground

D. Merk et al.

Title Page

Abstract

Introduction

Conclusions

References

Tables

Figures



Back

Close

Full Screen / Esc

Printer-friendly Version

Interactive Discussion



## Cloud properties from satellite and ground

D. Merk et al.

Title Page

Abstract

Introduction

Conclusions

References

Tables

Figures



Back

Close

Full Screen / Esc

Printer-friendly Version

Interactive Discussion



et al., 2006; Bennartz, 2007). Therefore it is important to investigate its validity. The comparison of  $N_d$  and  $H_{\text{cloud}}$  from both space and ground has not yet been carried out although Placidi et al. (2007) pointed out that their combined retrieval would give the opportunity to derive the first indirect effect with high spatial and temporal resolution.

The validation of retrieved  $N_d$  and  $H_{\text{cloud}}$  from passive sensing satellite instruments remains a challenging task. In this study, we contrast such satellite retrievals with the same cloud parameters retrieved independently from ground-based remote sensing.

Remote sensing methods from ground are able to provide reliable detection of cloud geometric borders through the combination of ceilometer and radar (Boers et al., 2000; Shupe, 2007; Illingworth et al., 2007; Martucci et al., 2010). Several retrieval methods have been developed over the last years combining different instruments or exploiting novel techniques to retrieve information about the vertical microphysical structure of the cloud. Given only the cloud radar measurements, a common approach is to relate liquid water content with the radar reflectivity via a power-law relationship. A short overview of studies applying such methods is given in Löhnert et al. (2001). With additional measurements by a microwave radiometer, more accurate retrievals of  $q_L$  (e.g. Frisch et al., 1998; Dong and Mace, 2003) and even  $N_d$  become possible. Rémillard et al. (2013) suggests a radar-radiometer retrieval of  $N_d$  based on a condensational growth model taking the vertical velocity into account and allowing small variations of  $N_d$  with height, while it is assumed vertically constant in most other studies. Accompanying lidar extinction measurements have been used to retrieve  $q_L$ , effective radius ( $r_e$ ) and  $N_d$  in parallel (Martucci and O'Dowd, 2011), although the fast extinction within the first few decameters of the cloud. Also observation of solar radiation can be included as additional independent information (Dong et al., 1997, 2002). Recently, a technique to derive profiles of  $q_L$ ,  $r_e$ , and  $N_d$  was developed based on measurements with dual-field-of-view (DFOV) Raman lidar (Schmidt et al., 2013). The amplitude of the aerosol cloud interaction was investigated similar to the approach presented by Feingold et al. (2003) by relating the measured aerosol extinction coefficient below cloud base to the retrieved cloud microphysical properties of the same profile. Taking co-located Doppler

lidar measurements of vertical velocity into account, it was found that for small temporal and spatial scales the strength of updrafts considerably determines the intensity of the aerosol cloud interaction especially at cloud base (Schmidt et al., 2014a). On large spatial and temporal scales and in the cloud-top region the impact of up- and downdrafts on the aerosol cloud interaction levels out and approaches values similar to those obtained from measurements of passive spaceborne sensors (Schmidt et al., 2014b). At this time, the DFOV Raman lidar technique can only be applied during nighttime, which hinders its application for the evaluation of measurements by spaceborne sensors such as SEVIRI or MODIS that rely on daylight conditions for the retrieval of liquid-cloud microphysical properties.

Our aim is to gain a better understanding of the current possibilities and shortcomings when these key quantities of clouds are retrieved, by simultaneously adopting the space and ground perspective, and by contrasting them to each other. Due to the under-constrained nature and assumptions made in retrieval methods, substantial differences for the obtained microphysical parameters may occur, as pointed out by Turner et al. (2007), who investigated several ground-based retrieval methods for one case study of ground-based observations. We use a synergistic dataset combining SEVIRI, MODIS and Cloudnet (Illingworth et al., 2007) to address these problems. We investigate how close the adiabatic assumption matches the observations from ground and if the satellite retrievals can benefit from information about cloud adiabaticity retrieved from the ground.

The paper is structured as follows. In Sect. 2, we describe the instruments and data processing tools and algorithms used within this study. The retrieval methods based on an adiabatic description of clouds are presented in Sect. 3. Therein also a new optimal estimation retrieval of  $N_d$  using ground-based radar and microwave radiometer are presented. In Sect. 4 these retrievals are applied to four different cases which are then used to evaluate the satellite-based observations. Finally, a conclusion and outlook is given in Sect. 5.

## Cloud properties from satellite and ground

D. Merk et al.

Title Page

Abstract

Introduction

Conclusions

References

Tables

Figures



Back

Close

Full Screen / Esc

Printer-friendly Version

Interactive Discussion



## 2 Data

### 2.1 Instruments and retrievals

For our study we combine observations from SEVIRI (Spinning Enhanced Visible and InfraRed Imager) onboard Meteosat Second Generation (MSG) and MODIS (Moderate-Resolution Imaging Spectroradiometer) onboard Terra and Aqua with ground-based remote sensing data obtained with the same mobile instruments at sites at Leipzig, Germany (51.35° N, 12.43° E) and during a three month campaign at Krauthausen, Germany (50.897° N, 6.46° E).

Data from SEVIRI (Schmetz et al., 2002) are used for the geostationary satellite perspective. SEVIRI provides 12 spectral channels covering the visible, the near infrared, and the infrared spectrum. The channels used here have a nadir resolution of 3 km × 3 km. The spatial resolution decreases towards the poles and is about 4 km × 6 km over our region of interest (Central Europe). In this study we use the 5 min temporal resolution data from the Rapid Scan Service (RSS). The SEVIRI radiances in the different channels are used as input for the Nowcasting Satellite Application Facility (NWCSAF) algorithm (Derrien, 2012) which provides a cloud mask, cloud top height, and cloud classification.

This cloud mask is used for deriving cloud phase, cloud optical depth, and effective radius with the KNMI cloud physical properties (CPP) algorithm (Roebeling et al., 2006), developed in the context of satellite application facility on climate monitoring (CMSAF, Schulz et al., 2009). To derive the cloud mask different multispectral tests using SEVIRI channels are applied in order to discriminate cloudy from cloud-free pixels. The cloud top height for low, liquid clouds is obtained by using a best fit between measured brightness temperatures in the 10.8 μm channel and simulated values using the RTTOV radiative transfer model (Saunders et al., 1999) applied to atmospheric profiles from the ECMWF NWP model. Using a channel in the visible spectrum (0.6 μm) together with an absorbing channel in the near infrared (1.6 μm) (Nakajima and King, 1990), the CPP algorithm retrieves cloud optical depth as well as effective radius which

### Cloud properties from satellite and ground

D. Merk et al.

Title Page

Abstract

Introduction

Conclusions

References

Tables

Figures



Back

Close

Full Screen / Esc

Printer-friendly Version

Interactive Discussion



are representative for the uppermost cloud part. As this method relies on solar channels it works only during daytime.

MODIS is an imaging spectrometer onboard Terra (descending node) and Aqua (ascending node) which probe the Earth's atmosphere from a polar orbit that results in one daytime overpass per satellite per day over the region of interest. MODIS measures in 36 bands in the visible, near-infrared, and infrared spectrum, with some bands having a spatial resolution of up to 250 m. The cloud physical properties (Platnick et al., 2003) are retrieved in a similar manner as for SEVIRI, but at 1 km spatial resolution using the channels 0.6  $\mu\text{m}$  (band 1) over land and 2.1  $\mu\text{m}$  (band 7). In addition, effective radius retrievals are available using the channels at 1.6  $\mu\text{m}$  (band 6) and 3.7  $\mu\text{m}$  (band 20) together with band 1. Note that band 6 on the Aqua satellite suffers from a stripe-problem (Meirink et al., 2013). In this study MODIS collection 5.1 is used for the retrieved cloud optical depth and effective radius.

The ground remote sensing instruments of the Leipzig Aerosol and Cloud Remote Observations System (LACROS) comprise a 35 GHz MIRA cloud radar, a HATPRO microwave radiometer, and a CHM15X ceilometer, which are used also for field campaigns. All instruments are operated in a vertically pointing mode. The raw measurements are processed with the Cloudnet algorithm package (Illingworth et al., 2007). The output data is available in an unified temporal resolution of 30 s and a vertical grid of 30 m. Cloudnet uses further information from a numerical weather prediction (NWP) model (here: COSMO-DE). In this study we use the attenuation-corrected radar reflectivity from the cloud radar, together with its error estimate, the liquid water path obtained from the microwave radiometer, as well as the cloud base and top height retrieved from ceilometer and cloud radar, respectively. Also the vertical Doppler velocity from the cloud radar is utilized. Furthermore Cloudnet provides a target classification applying a series of tests to discriminate cloud phase, drizzle or rain, and aerosols or insects.

Cloud properties from satellite and ground

D. Merk et al.

Title Page

Abstract

Introduction

Conclusions

References

Tables

Figures



Back

Close

Full Screen / Esc

Printer-friendly Version

Interactive Discussion



## 2.2 Synoptic conditions

For this study, we focus on ideal cases to gain a better understanding of the microphysical processes within the cloud by ruling out side-effects accompanying complicated cloud scenes as good as possible. We picked time periods for several days in a way that the most interesting cloud deck was covered by all ground instruments as well as by MODIS and SEVIRI. Ideal cases are single-layer cloud systems which are entirely liquid and non-drizzling. For this study we selected two rather homogeneous cases (27 October 2011 and 21 April 2013), and two more inhomogeneous cases (1 June 2012, 27 September 2012) in time which were observed by the instruments from LACROS at either Leipzig or Krauthausen. A short overview of the characteristics is given in Table 1. The cloud boundaries are shown along with the cloud radar reflectivity profile in Fig. 1. In the following we describe the synoptic conditions for each case.

A high pressure system dominates the synoptic weather pattern on 27 October 2011 (Fig. 1a). The temperature at the 850 hPa pressure level over Leipzig is around 5°C. Therefore the stratocumulus cloud layer that is observed between 10:30 and 13:00 UTC consists entirely of water droplets. Its geometrical depth increases in the beginning of the observation period. The Cloudnet classification indicates a cloud deck even before (not shown), although the radar is not sensitive enough to detect the thin cloud layer between 10:00 and 10:30 UTC.

The weather pattern on 21 April 2013 (Fig. 1b) is quite similar with the high pressure influence being stronger. The temperatures at the 850 hPa pressure level are slightly positive. During the whole observation period at Krauthausen a closed cloud deck is visible. The ground-obtained cloud top height shows only small variability, while the cloud base is more inhomogeneous during the beginning of the observation period. A thin overlying Cirrus cloud deck can be observed around 10:00 and between 11:00–12:00 UTC.

An upper-level ridge covers Central Europe on 1 June 2012 (Fig. 1c), but the area around Leipzig is also influenced by a surface low. Temperatures at 850 hPa lie around

Title Page

Abstract

Introduction

Conclusions

References

Tables

Figures



Back

Close

Full Screen / Esc

Printer-friendly Version

Interactive Discussion



10°C. The stratocumulus cloud deck with the cloud tops slightly below 2000 m between 12:00 and 16:00 UTC is broken with some cloudy periods in the early afternoon that are not well detected by the cloud radar.

The weather pattern for the 27 September 2012 (Fig. 1d) shows Leipzig directly in front of a well pronounced trough. Temperatures at 850 hPa lie again around 10°C and the cloud types vary between stratocumulus and shallow cumulus. The cloud base height increases throughout the day. After 16:00 UTC also some precipitation can be observed for a short time by means of virga that did not reach the ground.

### 3 Cloud microphysical retrieval methods

To investigate aerosol indirect effects from satellite the adiabatic cloud model is commonly applied in state-of-the-art retrievals. It describes the distribution of microphysical parameters within the cloud. In this section we present the background of the adiabatic model, followed by a description of the retrieval methods applied in this study.

#### 3.1 Adiabatic cloud model

The behavior of a rising moist air parcel can be described as an adiabatic process if no entrainment takes place. Above the lifted condensation level, condensation begins and droplets start to grow with height. Condensation provides additional liquid water that is distributed over the number of droplets ( $N_d$ ) in the volume. The liquid water content profile  $q_L(z)$  increases linearly with height (Albrecht et al., 1990) and can be related to  $N_d(z)$  and the mean volume droplet radius  $r_v(z)$ :

$$q_L(z) = \Gamma_{ad}(T, p)z = \frac{4}{3}\pi r_v^3(z)\rho_w N_d(z) \quad (1)$$

Here  $z$  is the height above cloud base,  $\rho_w$  is the density of water and  $\Gamma_{ad}(T, p)$  describes the adiabatic liquid water content gradient as a function of temperature and

Title Page

Abstract

Introduction

Conclusions

References

Tables

Figures



Back

Close

Full Screen / Esc

Printer-friendly Version

Interactive Discussion



pressure. Restructuring this relationship and considering  $N_d$  constant with height yields the following mean cloud droplet radius profile ( $r_v(z)$ ):

$$r_v(z) = \left( \frac{3\Gamma_{ad}(T, \rho)}{4\pi\rho_w N_d} \right)^{1/3} z^{1/3} \quad (2)$$

In remote sensing the effective radius ( $r_e$ ) is more relevant, as it can be obtained from reflected solar radiation measurements. The effective radius is defined as the third over the second moment of the droplet size distribution (Hansen and Travis, 1974) and can be linked to the mean volume radius ( $r_v$ ) with the following relationship:

$$r_e^3(z) = k^{-1} r_v^3(z) \quad (3)$$

The factor  $k$  depends on the cloud type and corresponding typical droplet size distributions. Typical values for marine and continental liquid water clouds are 0.67 and 0.80, respectively (Brenguier et al., 2000).

Deviations from a pure adiabatic cloud can be accounted for by replacing  $\Gamma_{ad}(T, \rho)$  by  $\Gamma_{eff} = \Gamma_{ad}(T, \rho)f_{ad}(z)$ , introducing the so-called adiabatic factor  $f_{ad}(z)$ . It can have values between 0 and 1, where a pure adiabatic cloud would correspond to  $f_{ad} = 1$ . The deviation from the pure adiabatic  $q_L$  profile can result from mixing with dry air by either reducing the  $N_d$  (inhomogeneous mixing), reducing the radius (homogeneous mixing) or a mixture of both processes (Lehmann et al., 2009). In general, for the adiabatic factor  $f_{ad}(z)$  a range of [0.3, 0.9] is seen as common (Boers et al., 2006). In the following we assume  $f_{ad}(z)$  to be constant for the whole vertical profile and write it as  $f_{ad}$ .

### 3.2 Satellite retrievals

The adiabatic model can be used to relate  $Q_L$  (Eq. 4),  $N_d$  (Eq. 5) as well as the adiabatic cloud depth  $H_{ad}$  (Eq. 6) to the effective radius ( $r_e$ ) and optical depth ( $\tau$ ). The latter two

Cloud properties from satellite and ground

D. Merk et al.

Title Page

Abstract

Introduction

Conclusions

References

Tables

Figures



Back

Close

Full Screen / Esc

Printer-friendly Version

Interactive Discussion



can be retrieved from satellite remote sensing using the method described in Nakajima and King (1990):

$$Q_L^{\text{SEVIRI}} = \frac{5}{9} \rho_w \tau r_e \quad (4)$$

$$N_d^{\text{SEVIRI}} = A_1 \tau^{0.5} r_e^{-2.5} \quad (5)$$

$$H_{\text{ad}}^{\text{SEVIRI}} = A_2 \tau^{0.5} r_e^{0.5} \quad (6)$$

These equations are also applied for MODIS  $\tau$  and  $r_e$ . The factors  $A_1$  and  $A_2$  are variable (Janssen et al., 2011). They depend on  $\Gamma_{\text{ad}}(T, \rho)$  and the adiabatic factor. Often they are considered to be constant. In doing so pure adiabatic clouds with a representative  $\Gamma_{\text{ad}}(T, \rho)$  are assumed (e.g. Quaas et al., 2006). The uncertainty of the different parameters contained in  $A_1$  are discussed by Janssen et al. (2011). They estimated the uncertainty of  $k$  to be negligible (around 3%). When considering the whole seasonal variability of cloud base temperature, they obtained an error of 24 % for the adiabatic lapse rate of liquid water mixing ratio ( $\Gamma_{\text{ad}}(T, \rho)$ ). In our case, this error is supposed to be considerably smaller since we use NWP data to constrain the cloud top temperature. Janssen et al. (2011) were further assuming an uncertainty in the adiabatic factor of 0.3. This resulted in a numerically evaluated error of around 26 % considering typical values of effective radius and optical depth. We will discuss the applicability and shortcomings of the adiabatic model in Sect. 4.

### 3.3 Ground-based retrievals

Ground-based retrievals usually combine several remote sensing techniques. From the ceilometer extinction profile it is possible to obtain the cloud base height, because the laser beam is strongly attenuated by liquid droplets and photons are only able to penetrate the lowest part of the cloud (Martucci et al., 2010). The radiation of the cloud radar is, on the other hand, able to penetrate clouds and the strong gradient of the range-corrected radar reflectivity profile is used to determine the cloud top height.

Title Page

Abstract

Introduction

Conclusions

References

Tables

Figures



Back

Close

Full Screen / Esc

Printer-friendly Version

Interactive Discussion



## Cloud properties from satellite and ground

D. Merk et al.

Title Page

Abstract

Introduction

Conclusions

References

Tables

Figures



Back

Close

Full Screen / Esc

Printer-friendly Version

Interactive Discussion



For the derivation of the cloud top we further use the Cloudnet target classification, so that the cloud top and base heights refer only to the liquid cloud layer and ignore overlaying cirrus clouds. This difference between cloud top and cloud base height is referred to as the observed cloud geometrical depth ( $H_{\text{obs}}^{\text{ground}}$ ). The adiabatic scaled

cloud depth ( $H_{\text{ad}}^{\text{ground}}$ ) is obtained by assuming a linear  $q_L$  profile which integral matches the observed  $Q_L$  from the microwave radiometer, starting from the cloud base while accounting for  $\Gamma_{\text{ad}}(T, \rho)$  at cloud base:

$$H_{\text{ad}}^{\text{ground}} = \sqrt{2 \cdot \frac{Q_L}{\Gamma_{\text{ad}}(T, \rho)}} \quad (7)$$

To calculate the adiabatic factor ( $f_{\text{ad}}$ ) we relate the  $H_{\text{obs}}^{\text{ground}}$  to  $Q_L$  obtained from the microwave radiometer (Wood, 2006).

$$f_{\text{ad}} = \frac{2Q_L}{\left(H_{\text{obs}}^{\text{ground}}\right)^2 \Gamma_{\text{ad}}(T, \rho)} \quad (8)$$

Cloud microphysical quantities can be described in terms of moments of the droplet size distribution. The cloud droplet number concentration is equivalent to the zeroth moment, the mean radius to the first moment, the liquid water content is proportional to the third moment, while the effective radius is the third over the second moment and the radar reflectivity factor is proportional to the sixth moment. Relating these moments gives the chance to fully describe a unimodal distribution following either a gamma or lognormal shape and therefore calculating other moments of the size distribution which are not directly observed (Rémillard et al., 2013). This is the basis for most retrieval methods. In the next section, we present a retrieval combining microwave radiometer and cloud radar observations, followed by a description of two optimal estimation approaches. These use the same observations but also account for the instrument uncertainties and prior assumptions of adiabatic liquid cloud profiles.

Given  $H_{\text{obs}}^{\text{ground}}$  and  $N_{\text{d}}^{\text{OE1}}$  (described in the following Sect. 3.3.2) we can calculate the ground-based optical depth ( $\tau^{\text{ground}}$ , Eq. 9) and effective radius ( $r_{\text{eff}}^{\text{ground}}$ , Eq. 10) (Wood, 2006) which are also used for comparison with the satellite obtained values later on.

$$\tau^{\text{ground}} = 0.0145 \cdot (\Gamma_{\text{ad}}(T, \rho) f_{\text{ad}})^{\frac{2}{3}} \left( k N_{\text{d}}^{\text{OE1}} \right)^{\frac{1}{3}} \left( H_{\text{obs}}^{\text{ground}} \right)^{\frac{5}{3}} \quad (9)$$

$$r_{\text{e}}^{\text{ground}} = 0.0620 \cdot (\Gamma_{\text{ad}}(T, \rho) f_{\text{ad}})^{\frac{1}{3}} \left( k N_{\text{d}}^{\text{OE1}} \right)^{-\frac{1}{3}} \left( H_{\text{obs}}^{\text{ground}} \right)^{\frac{1}{3}} \quad (10)$$

### 3.3.1 Radar-radiometer retrieval of cloud droplet number concentration

Following Fox and Illingworth (1997), we relate the measured radar reflectivity ( $Z$ ),  $q_{\text{L}}$  and  $N_{\text{d}}$ . Thereby it is assumed that the droplet size distribution can be described by a gamma distribution with index  $\beta$  (Fox and Illingworth, 1997; Martucci and O'Dowd, 2011). A similar method has been applied in (Rémillard et al., 2013), but using a log-normal size distribution. Although  $N_{\text{d}}$  may vary vertically, it is commonly suspected that it stays nearly constant throughout the vertical column of a nonprecipitating cloud (Bennartz, 2007; Brenguier et al., 2000). To retrieve the column cloud droplet number concentration from the available single-layer observations, we integrate  $q_{\text{L}}$  over the cloud column and can therefore use  $Q_{\text{L}}$  from the microwave radiometer (compare Rémillard et al., 2013):

$$N_{\text{d}}^{\text{FI}} = \frac{9}{2\pi^2 k \rho^2} \frac{(\beta + 6)!}{(\beta + 3)! (\beta + 3)^3} \frac{Q_{\text{L}}^2}{\left( \int \sqrt{Z} dz \right)^2} \quad (11)$$

Both, homogeneous and inhomogeneous mixing (Lehmann et al., 2009) can easily alter the microphysical quantities in clouds in ways not adequately addressed within the retrieval schemes. For example, the size distribution may become skewed and not be accurately described with a gamma-shape anymore. However, Boers et al. (2006) and Janssen et al. (2011) found out, that both assumptions about the mixing process result in nearly the same vertically averaged  $N_{\text{d}}$ .

Title Page

Abstract

Introduction

Conclusions

References

Tables

Figures

◀

▶

◀

▶

Back

Close

Full Screen / Esc

Printer-friendly Version

Interactive Discussion



### 3.3.2 Optimal Estimation of cloud droplet number concentration

The Optimal Estimation (OE) technique allows to derive the cloud droplet number concentration and the liquid water content profile considering also observation uncertainties. We introduce here two different strategies in order to better address the topic of cloud adiabacity.

Both approaches are based on the assumptions mentioned above, i.e. a vertically constant  $N_d$ , a gamma-shaped droplet size distribution with parameter  $\beta$  and a nonlinear relationship between  $q_L$ ,  $N_d$ , and  $Z$ . We include error estimates for the observed quantities as well as an a-priori state together with its error estimate. The optimal estimation method aims on finding the most likely state given the observations. Therefore we try to minimize a cost function following Rodgers (2000).

The main difference of the two approaches lies in the degree of freedom for the  $q_L$  profile. For the first method, we allow the  $q_L$  profile to take any shape and therefore deviate from the adiabatic model (referred to as OE1), while the second method enforces a linear increase of  $q_L$  with height (OE2). The cost function of OE2 can thus be used as a measure of deviation from the adiabatic assumption.

Our observation vector ( $\mathbf{y}$ ) for OE1 contains the radar reflectivity  $Z$  and the microwave radiometer  $Q_L$ . Our state vector ( $\mathbf{x}$ ) for OE1 contains the vertically-constant  $N_d$  and the natural logarithm of the vertical  $q_L$  profile. The logarithm is used to avoid the occurrence of unphysical negative liquid water contents in the minimization process.

$$\mathbf{y} = (Z, Q_L)^T; \quad \mathbf{x} = (N_d, \ln(q_L))^T \quad (12)$$

The forward model ( $F(\mathbf{x})$ ) for OE1 consists of two separate parts: a model  $H_1$  (Eq. 13) for the calculation of  $Q_L$ , and a model  $H_2$  (Eq. 11) for the calculation of  $N_d$  given the state vector  $\mathbf{x}$ .

$$H_1 : Q_L = \int \exp(\ln(q_L(z))) dz \quad (13)$$

Title Page

Abstract

Introduction

Conclusions

References

Tables

Figures

◀

▶

◀

▶

Back

Close

Full Screen / Esc

Printer-friendly Version

Interactive Discussion



The main difference for OE2 lies in the state vector, which does not contain the  $q_L$  profile since this is fixed by the observation of  $Q_L$  using the adiabatic scaled  $q_L$  profile.

$$\mathbf{x} = (N_d)^T \quad (14)$$

The observation vector remains the same (Eq. 12). The forward model for OE2 only consists of the  $N_d$  calculation in the same way as for OE1 (Eq. 11).

The Jacobians are calculated numerically using finite differences for both methods as follows:

$$H(x) = \frac{\delta y_j}{\delta x_j} = \frac{F(x_j + dx_j) - F(x_j)}{dx_j} \quad (15)$$

We apply the Levenberg-Marquardt minimization method until convergence is reached (Hewison, 2007). Only profiles with all required input data was processed. Only 0.1 % failed convergence within 30 iteration steps.

For the prior state vector of OE1 we assume that the liquid water profile follows the adiabatic scaled profile. For OE2 the  $q_L$  profile is always set equal to the adiabatic scaled profile. For the a-priori  $N_d$  we set a value of  $300 \text{ cm}^{-3}$  which is a typical value for continental sites (Miles et al., 2000). We assume that there are no correlations between the elements in the covariance matrix, implying no correlations of the  $q_L$  uncertainties at different height levels and no correlations between  $q_L$  and  $N_d$  uncertainties. This is a rather simplistic assumption, but the variances are set reasonably large. The SD for  $N_d$  is set to  $300 \text{ cm}^{-3}$  and for  $\ln(q_L)$  to  $2.5 \ln(\text{gm}^{-2})$ .

Just as for the background error covariance matrix, we assume for the observation error covariance matrix that there is no cross-correlation, and that all off-diagonal terms are thus zero.

The observation error covariance could be split up into individual contributing parts such as forward model error, radiometric noise error, and representativeness error. Here only forward model errors and the observation errors are considered. Observation errors are given by the Cloudnet algorithm. The forward model error is estimated by

Cloud properties from satellite and ground

D. Merk et al.

Title Page

Abstract

Introduction

Conclusions

References

Tables

Figures



Back

Close

Full Screen / Esc

Printer-friendly Version

Interactive Discussion



applying values of  $\beta$  in the range of 1 to 6 to the radar forward model and taking the variance of the resulting reflectivity values for a sample cloud profile with a geometrical extent of 700 m and linearly increasing  $q_L$  in steps of  $0.1 \text{ g m}^{-2}$  per 100 m.

## 4 Results

5 The retrieval methods described in the previous section have been applied to the case studies introduced in Sect. 2.2. We investigate differences for cloud key parameters for four cases, two being more homogeneous and two showing more temporal variability in cloud cover. Those key parameters are important for further investigation of the first indirect effect. Deviations resulting from two different perspectives on the same cloud scene have to be kept in mind for the interpretation.

### 4.1 Retrieval of cloud properties from ground

We first evaluate the results from the ground-based perspective before comparing those to the satellite retrieved values.

#### 4.1.1 Cloud geometrical depth and cloud adiabacity

15 From ground we have the opportunity to compare  $H_{\text{obs}}^{\text{ground}}$  observed with radar and lidar with the virtual adiabatic  $H_{\text{ad}}^{\text{ground}}$  derived from  $Q_L$  measurements (Eq. 7).

Differences between  $H_{\text{obs}}^{\text{ground}}$  and  $H_{\text{ad}}^{\text{ground}}$  can be mainly explained by subadiabaticity (Roebeling et al., 2008a). Entrainment of dry air leads to deviations from the linearly increasing  $q_L$  profile. The cloud adiabatic factor as calculated from Eq. (8) using  $Q_L$  from the microwave radiometer and  $H_{\text{obs}}^{\text{ground}}$  can quantify such deviations.

20 Comparing the time series of  $H_{\text{obs}}^{\text{ground}}$  and  $H_{\text{ad}}^{\text{ground}}$  for the two homogeneous cases (Fig. 2a and b), we find a correlation of 0.96 on 27 October 2011. For 21 April 2013 we find a correlation of 0.56 after 09:00 UTC. Before 09:00 UTC the adiabatic scaled

cloud depth is considerably smaller than the values obtained by the observed cloud depth. The radar reflectivity measurements (Fig. 1b) reveal that the cloud base is more inhomogeneous during this time period than later on. On average,  $H_{\text{obs}}^{\text{ground}}$  is larger than  $H_{\text{ad}}^{\text{ground}}$ , 284 m versus 238 m for 27 October 2011, and 404 m vs. 313 m for 21 April 2013.

The time series of the adiabatic factor calculated for the two homogeneous cases is shown in Fig. 3a and b. The adiabatic factor at 27 October 2011 lies in the range from 0.4 to 0.9. Short time periods with  $f_{\text{ad}} > 1$  occur. These superadiabatic points are likely to be artefacts, since the occurrence of superadiabatic cloud profiles in nature is physically implausible. Such artefacts may arise due to enhanced  $Q_{\text{L}}$  by drizzle or an underestimation of actual  $H_{\text{cloud}}$ . In contrast to the original Cloudnet code, our calculation of the adiabatic factor allows for values greater than one. Within Cloudnet superadiabatic profiles are avoided by increasing the cloud top height if the adiabatic integrated  $q_{\text{L}}$  is smaller than  $Q_{\text{L}}$  measured by the microwave radiometer. We omitted adiabatic factors with  $f_{\text{ad}} > 1.5$  since we believe that those are most likely affected by the measurement uncertainties. At 21 April 2013 we find values between 0.2 and 0.6 before 09:00 UTC corresponding to the larger  $H_{\text{obs}}^{\text{ground}}$ . After 09:00 UTC the adiabatic factor oscillates between 0.5 and 1.0. Overall, the adiabatic factors found for the homogeneous cases agrees well with the range of values of [0.3, 0.9] suggested by Boers et al. (2006).

For the two inhomogeneous cases (Fig. 2c and d) we find correlations between  $H_{\text{obs}}^{\text{ground}}$  and  $H_{\text{ad}}^{\text{ground}}$  of 0.63 (1 June 2012) and 0.76 (27 September 2012). Similar to the homogeneous cases, we see that  $H_{\text{obs}}^{\text{ground}}$  points to thicker clouds in general. The mean of  $H_{\text{obs}}^{\text{ground}}$  is 364 m in contrast to the mean of  $H_{\text{ad}}^{\text{ground}}$  which is 244 m for 1 June 2012 and 314 m in contrast to 261 m for 27 September 2012.

For the two inhomogeneous cases the variability of the adiabatic factor (Fig. 3c and d) is larger than for the homogeneous cases considered before (Table 3), but the range

Cloud properties  
from satellite and  
ground

D. Merk et al.

Title Page

Abstract

Introduction

Conclusions

References

Tables

Figures



Back

Close

Full Screen / Esc

Printer-friendly Version

Interactive Discussion



of values is similar. This shows that independent from cloud homogeneity many clouds are actually subadiabatic.

We are furthermore interested in dependencies of the adiabatic factor on the cloud morphology and thermodynamics. For the following investigation, we consider data points from all four cases. We relate the adiabatic factor to  $H_{\text{obs}}^{\text{ground}}$  and the median radar-observed vertical velocity of each cloud layer.

Figure 4 reveals a tendency that geometrical thicker clouds are less adiabatic, while mainly the thin clouds ( $H_{\text{obs}}^{\text{ground}} < 400\text{m}$ ) are responsible for the superadiabatic cloud profiles. The investigation of such thin clouds remains challenging. This can be seen also when considering the uncertainties that influence the adiabatic factor. For example, consider a cloud with  $Q_L = 100\text{g m}^{-2}$  and  $H_{\text{obs}}^{\text{ground}} = 324\text{m}$  that is purely adiabatic ( $f_{\text{ad}} = 1$ ). The  $Q_L$  retrieval uncertainty (microwave radiometer instrument error + retrieval error) lies around  $20\text{g m}^{-2}$  and the  $H_{\text{obs}}^{\text{ground}}$  uncertainty is at least  $\pm 60\text{m}$  due to the vertical resolution. Accounting for the maximum uncertainty ( $Q_L = 120\text{g m}^{-2}$ , and  $H_{\text{obs}}^{\text{ground}} = 264\text{m}$ ) or ( $Q_L = 80\text{g m}^{-2}$  and  $H_{\text{obs}}^{\text{ground}} = 384\text{m}$ ), the resulting adiabatic factor would be 1.81 or 0.57, respectively. This shows that with the current uncertainty limits of the ground-based observations the adiabatic factor is still prone to large uncertainties.

The average vertical velocity of each cloud profile is found at  $-0.1\text{ m s}^{-1}$  with the majority of points in the range  $[-1, 1]\text{ m s}^{-1}$ . Considering this vertical velocity as function of cloud adiabacity we find a large spread, which makes it difficult to detect a clear dependence of cloud adiabacity on updraft speed. However if we calculate the median adiabatic factor for the updraft and downdraft regimes individually, we find for each of our case studies that the clouds are slightly more adiabatic in the updraft regime (Table 3). This behaviour is expected from adiabaticity and also supported by the findings of e.g. Schmidt et al. (2014a). They used observations of two cases with homogeneous stratocumulus clouds over Leipzig, Germany, and observed that in case of updrafts in the clouds, the  $q_L$  profile is more adiabatic. They also report that this effect is strongest

## Cloud properties from satellite and ground

D. Merk et al.

Title Page

Abstract

Introduction

Conclusions

References

Tables

Figures



Back

Close

Full Screen / Esc

Printer-friendly Version

Interactive Discussion



at the cloud base and blurs when the data points are averaged over the whole cloud profile.

#### 4.1.2 Cloud droplet number concentration

$N_d$  is used as the main parameter in many investigations of the first indirect aerosol effect. Advances have been made over the last two decades to apply retrievals for  $N_d$  combining ground-based cloud radar and microwave radiometer. We applied such a method following Fox and Illingworth (1997) (hereafter: FI, see Sect. 3.3.1). Furthermore we compare those results with the newly developed Optimal Estimation approaches (see Sect. 3.3.2).

Contrasting the  $N_d$  from OE1 and OE2 with the FI method, we find that the absolute mean difference of  $N_d^{OE1}$  and  $N_d^{FI}$  considering all cases is smaller with  $164 \text{ cm}^{-3}$  (19 %) than for  $N_d^{OE2}$  and  $N_d^{FI}$  with  $271 \text{ cm}^{-3}$  (31 %). Overall, the FI method tends to yield lower values than the OE1 method, even though some outliers with unreasonable large values can be found ( $N_d^{OE1} > 2000 \text{ cm}^{-3}$ ). Outliers also occur for OE2, but can be filtered using the cost function. Neglecting  $N_d$  retrievals with cost function values greater than 2, we find a correlation between OE1 and OE2 of 93%. In contrast to the FI method the OE methods are also able to give information about the remaining uncertainty by processing measurement uncertainties as well as the uncertainty of the background state. With a quite large background uncertainty assumed to be  $300 \text{ cm}^{-3}$ , we can see that the information (measurement and uncertainties) from the ground observation is able to reduce the final analysis error for  $N_d$ , but more constraints are required to obtain  $N_d$  with even higher accuracy. This would be desirable to better evaluate satellite observations.

To investigate the two OE approaches in more detail, we compared them in terms of the remaining cost function ( $J$ ) of the OE2 approach that allows only adiabatic profiles. As shown in Fig. 5 the agreement of  $N_d$  especially for the two homogeneous cases is close for values smaller than  $300 \text{ cm}^{-3}$  and  $J < 2$ . Increasing the cost function leads

### Cloud properties from satellite and ground

D. Merk et al.

Title Page

Abstract

Introduction

Conclusions

References

Tables

Figures



Back

Close

Full Screen / Esc

Printer-friendly Version

Interactive Discussion



to a steady disagreement of the  $N_d^{\text{OE1}}$  and  $N_d^{\text{OE2}}$ . Furthermore  $N_d^{\text{OE2}}$  gives gradually higher values with increasing  $N_d$ . The first point can be interpreted as follows: the cost function remains high if it is not possible within the OE scheme to closely match the observations (i.e. the radar reflectivity profile). Since in the OE2 method an adiabatic profile is always required, higher cost function values can be interpreted as larger deviations of the observation from the adiabatic model if the assumption of a vertical constant CDNC is valid. For e.g. the 21 April 2013 case the deviations of the radar profile from the adiabatic description before 09:00 UTC can be clearly observed (compare Fig. 1b) in terms of a thin second layer occurring in the radar profiles closely below the base of the main layer. With a pure adiabatic description as applied for OE2 it is not possible to represent such a structure. This further confirms that even small deviations from the adiabatic assumption can lead to significant differences in the retrieval of key parameters used to investigate the first indirect aerosol effect.

## 4.2 Comparison of cloud properties from satellite and ground

Cloud microphysical retrievals that are based on either satellite or ground-based remote sensing both have their advantages and shortcomings. However, when the results of both approaches are in agreement, it is likely that the corresponding cloud layers are well suited for the investigation of key factors determining the first indirect effect.

By comparing ground-based and satellite observations, we have to consider the different spatial and temporal resolution, different error sources of the instruments as well as the different viewing zenith angle on the cloudy scene. For MSG SEVIRI we have to consider a parallax shift at higher latitudes. The satellite viewing zenith angle for Leipzig is  $58.8^\circ$ . Within this study the average cloud top height is between 1 and 3 km (see Table 1). This would result in a horizontal displacement of max. 5 km. Considering the spatial resolution of SEVIRI over Central Europe of  $4 \text{ km} \times 6 \text{ km}$ , we decided to neglect the parallax correction for our study. To address the uncertainty of the satellite

### Cloud properties from satellite and ground

D. Merk et al.

[Title Page](#)[Abstract](#)[Introduction](#)[Conclusions](#)[References](#)[Tables](#)[Figures](#)[Back](#)[Close](#)[Full Screen / Esc](#)[Printer-friendly Version](#)[Interactive Discussion](#)

## Cloud properties from satellite and ground

D. Merk et al.

Title Page

Abstract

Introduction

Conclusions

References

Tables

Figures



Back

Close

Full Screen / Esc

Printer-friendly Version

Interactive Discussion



observations from SEVIRI and also MODIS we calculated the SD of the surrounding pixels. For SEVIRI  $\pm 1$  pixel around the central pixel is added, resulting in a field of 9 satellite pixels. To cover a comparable area for MODIS, we add  $\pm 9$  pixel around the central pixel. For the comparison of the time series obtained from space and ground we applied data averaging only if mentioned. As pointed out in the following discussion for inhomogeneous scenes, omitting temporal averaging can lead to considerable differences of ground and satellite quantities.

### 4.2.1 Cloud geometrical depth

Contrasting  $H_{ad}^{SEVIRI}$  with the  $H_{obs}^{ground}$  from Cloudnet (Fig. 2), we are able to investigate the same quantity obtained with two independent physical retrieval approaches. The correlation is 0.44 for 21 April 2013 after 09:00 UTC, 0.59 for 27 October 2011, 0.44 for 1 June 2012, and 0.15 for 27 September 2012. The correlation increases when temporally averaging is applied (Table 2). The correlations for temporally averaged data are within the range that was also obtained by Roebeling et al. (2008a). They found correlations of 0.71 between SEVIRI and Cloudnet for a homogeneous stratocumulus cloud layer. The improvement of results is not surprising when comparing averaged data as also pointed out in other studies (Deneke et al., 2009). However, a too long averaging period could smear the original variability of the data.

Considering the mean difference of  $H_{ad}^{SEVIRI}$  and  $H_{ad}^{ground}$  for the homogeneous cases, we find values of 52 m (22 %) for 27 October 2011 (Fig. 2a) and 49 m (15 %) for 21 April 2013 (Fig. 2b). The temporal pattern is well captured by SEVIRI. As shown for 27 October 2011 in Fig. 6a, the largest differences in adiabatic cloud depth also show up as differences in  $Q_L$  between SEVIRI and Cloudnet as both differences are linearly linked and only depend on  $\Gamma_{ad}(T, p)$  (Eq. 7). Therefore differences in  $Q_L$  may be used as an indicator for agreement of cloud geometrical depth if only  $Q_L$  observations are available. On 27 October 2011 we find larger differences in  $Q_L$  after 12:00 UTC. The largest differences between  $H_{ad}^{SEVIRI}$  and Cloudnet  $H_{ad}^{ground}$  of around 200 m relate to  $Q_L$  differences

## Cloud properties from satellite and ground

D. Merk et al.

Title Page

Abstract

Introduction

Conclusions

References

Tables

Figures



Back

Close

Full Screen / Esc

Printer-friendly Version

Interactive Discussion



of  $100 \text{ g m}^{-2}$ . Although some slight drizzle beneath the cloud base is identified by the Cloudnet classification for several short time periods after 12:00 UTC, the drizzle signal in the radar reflectivity profile is not very pronounced (Fig. 1a). Generally drizzle could be a possible explanation for the higher  $Q_L$  observed with the ground-based microwave radiometer. The latter is sensitive to the total amount of liquid within the cloud, while the satellite retrieval is based on optical depth and effective radius in the uppermost cloud parts. Although the effective radius at both cloud base and cloud top is affected by drizzle, it has been previously observed that the former is more sensitive to drizzle (Chen et al., 2008). This can lead to biases in the different retrieval approaches for  $Q_L$ . The effective radius observed from satellite near cloud top lies clearly below the value of  $14 \mu\text{m}$  which was suggested by Rosenfeld et al. (2012) as the threshold to drizzle/rain forming clouds.

In the following, we contrast the behaviour of the two inhomogeneous cases (Fig. 2c and d) with the homogeneous cases (Fig. 2a and b). The mean differences between  $H_{\text{ad}}^{\text{SEVIRI}}$  and Cloudnet  $H_{\text{ad}}^{\text{ground}}$  are 116 m (47 %) and 103 m (39 %) for 1 June 2012 and 27 September 2012, respectively. Those values are twice as high as for the homogeneous cases. The  $Q_L$  obtained from the ground-based microwave radiometer is highly variable. Especially the Cloudnet observations at 27 September 2012 show rapid changes of  $Q_L$  with peaks around  $400 \text{ g m}^{-2}$  and cloud-free periods. The SEVIRI temporal pattern is more smooth, because the satellite signal represents an average over different sub-pixel clouds within the field of view. Within 10 min a cloud field advected at constant wind speed of  $10 \text{ m s}^{-1}$  over the ground site moves 6 km (spatial resolution of SEVIRI RSS). The comparison of such a 10 min averaged  $H_{\text{ad}}^{\text{SEVIRI}}$  and Cloudnet  $H_{\text{ad}}^{\text{ground}}$  gives mean differences of 119 m and 92 m for 1 June 2012 and 27 September 2012, respectively. Longer averaging times lead to slightly improved agreement. Averaging over 30 min results in mean differences of 101 m (44 %) and 68 m (27 %) for 1 June 2012 and 27 September 2012, respectively.

## 4.2.2 Cloud droplet number concentration

Also the retrieval of  $N_d$  from passive satellite observations relies on the adiabatic model. In the following we contrast  $N_d$  retrieved from ground with the OE1 method and the adiabatic retrieved values from MODIS and SEVIRI. We first consider the two homogeneous cases. The retrieved  $N_d$  is shown in Fig. 7a and b. At 21 April 2013 the values agree within the uncertainty range with a mean difference of  $78 \text{ cm}^{-3}$  (27%) between SEVIRI and OE1 retrievals for the whole time period.

At 27 October 2011 we find larger differences between SEVIRI and the ground-based retrievals. At the beginning of the observation period (before 10:30 UTC) the  $N_d^{\text{SEVIRI}}$  values are much lower than the  $N_d^{\text{OE1}}$  ones. After 10:30 UTC  $N_d^{\text{SEVIRI}}$  gives twice as large values as  $N_d^{\text{OE1}}$ , resulting in a mean difference of  $367 \text{ cm}^{-3}$  (116%) for the whole day.

To find explanations for the large deviations, we calculated optical depth and effective radius from  $N_d^{\text{OE1}}$  and  $H_{\text{obs}}^{\text{ground}}$  using the adiabatic model (Eqs. 9 and 10). By comparing these to the satellite-retrieved values we are able to attribute the observed differences mainly to differences in effective radius, for which SEVIRI gives lower values (Fig. 6). Before 10:30 UTC the mean difference of effective radius is  $2.5 \mu\text{m}$  compared to  $3.4 \mu\text{m}$  afterwards.  $Q_L$  differences can be attributed mainly to optical depth differences, which follows the same temporal pattern. Comparing the two satellite observations of the same cloud scene in the area of around  $\pm 100 \text{ km}$  around Leipzig (not shown), we find spatial inhomogeneities of cloud microphysics that can not be resolved in the same way by SEVIRI as it is possible for MODIS. Furthermore SEVIRI has to deal with a large solar zenith angle ( $> 60^\circ$ ) under relative azimuth angles close to  $180^\circ$  around noon, for which Roebeling et al. (2006) pointed out the lower precision of the CPP retrieval method.

Another influencing factor is the difference of effective radius retrieval due to the different channels used by MODIS ( $2.1 \mu\text{m}$ ) and SEVIRI ( $1.6 \mu\text{m}$ ) for the standard retrieval products. From MODIS, additional effective radius retrievals from channels at  $1.6 \mu\text{m}$

Title Page

Abstract

Introduction

Conclusions

References

Tables

Figures



Back

Close

Full Screen / Esc

Printer-friendly Version

Interactive Discussion



## Cloud properties from satellite and ground

D. Merk et al.

Title Page

Abstract

Introduction

Conclusions

References

Tables

Figures



Back

Close

Full Screen / Esc

Printer-friendly Version

Interactive Discussion



and  $3.7\ \mu\text{m}$  are available. Theoretically, the  $3.7\ \mu\text{m}$ -channel should represent the effective radius close to the cloud top for pure adiabatic clouds, while the  $2.1\ \mu\text{m}$ - and  $1.6\ \mu\text{m}$ -channels receive the main signal from deeper layers within the cloud. But real cloud observations do not always follow this relationship (Platnick, 2000; King et al., 2013). By comparing all available parallel observations of effective radius from MODIS and SEVIRI, we find the smallest mean absolute difference of effective radius of all channels between the SEVIRI  $1.6\ \mu\text{m}$ - and the MODIS  $1.6\ \mu\text{m}$ -channel with  $0.86\ \mu\text{m}$ . The difference increases when using the MODIS channels  $2.1\ \mu\text{m}$  and  $3.7\ \mu\text{m}$  to retrieve the effective radius. Intercomparison of MODIS channels only results in slightly smaller differences with  $0.68\ \mu\text{m}$  and  $0.51\ \mu\text{m}$  for MODIS  $2.1\ \mu\text{m}$  compared to  $1.6\ \mu\text{m}$  and  $3.7\ \mu\text{m}$  channels, respectively.

By considering the error propagation of the factor  $A_1$  and the optical depth in Eq. (5) for  $N_d$ , we find for 27 October 2011 at 11:45 UTC that the observed difference in effective radius of  $1.33\ \mu\text{m}$  between MODIS and SEVIRI results in an uncertainty of  $306\ \text{cm}^{-3}$ . The uncertainty due to differences in effective radius of  $0.34\ \mu\text{m}$  between MODIS channels  $2.1\ \mu\text{m}$  and  $1.6\ \mu\text{m}$  is  $57\ \text{cm}^{-3}$ .

Janssen et al. (2011) found for satellite retrievals of  $N_d$  (and also  $H_{\text{ad}}$ ) that  $f_{\text{ad}}$  and  $\Gamma_{\text{ad}}$  are important uncertainty factors. In our study  $\Gamma_{\text{ad}}$  has a smaller contribution to those uncertainties due to the fact that we are using model data to gain more reliable information about cloud top temperature and pressure instead of considering one constant value like in e.g. Quaas et al. (2006). To highlight the importance of considering the actual adiabatic factor for the retrieval process, we calculated the optical depth (Eq. 9) and effective radius (Eq. 10) from the ground-based observations using  $N_d^{\text{OE1}}$  and  $H_{\text{obs}}^{\text{ground}}$  with adiabatic factor  $f_{\text{ad}} = 1$  or the ground-obtained adiabatic factor. Afterwards we compare it to the satellite-retrieved values obtained with the CPP algorithm. When the adiabatic factor is assumed constant ( $f_{\text{ad}} = 1$ ) the mean difference in optical depth is 9.95 on 21 April 2013. When the adiabatic factor obtained from the ground-based measurements is considered, this mean difference is drastically reduced to 2.90. The mean difference of effective radius is reduced from 1.15 to  $0.12\ \mu\text{m}$ .

## Cloud properties from satellite and ground

D. Merk et al.

Title Page

Abstract

Introduction

Conclusions

References

Tables

Figures



Back

Close

Full Screen / Esc

Printer-friendly Version

Interactive Discussion



Therefore, we try to adjust  $N_d^{\text{SEVIRI}}$  for the homogeneous cases by multiplying with the adiabatic factor obtained from the ground-based observation. The results can be seen in Fig. 8. On 21 April 2013 the adjusted  $N_d^{\text{SEVIRI}}$  is generally slightly lower due to the observed subadiabaticity. Only before 09:00 UTC the adjustments leads to a better comparison to ground-obtained values. For 27 October 2011 the retrieved  $N_d^{\text{SEVIRI}}$  is also generally reduced, diminishing also the mean difference to the ground-retrieved values in this case. The reason that including the adiabatic factor does not generally lead to a better agreement can be attributed amongst other things to uncertainties of ground observations.

For the inhomogeneous cases shown in Fig. 7c and d, a high temporal variability in the optimal estimation retrievals of  $N_d$  can be seen.  $N_d^{\text{MODIS}}$  and the  $N_d^{\text{OE1}}$  agree well within the uncertainty range. For the comparison of  $N_d^{\text{SEVIRI}}$  and  $N_d^{\text{OE1}}$  we find good agreement in the beginning and end of the observation period at 1 June 2012 when the clouds are more homogeneous. Underestimation of  $N_d^{\text{OE1}}$  by SEVIRI during the more broken cloud scene can be mainly explained by a blending of the received signal from clouds and surface. The same explanation can also be applied to the second inhomogeneous case (27 September 2012). It remains open to which extent the inhomogeneity within a SEVIRI pixel destroys the reliability of retrieved parameters.

While some of the differences between satellite- and ground-based retrievals of  $N_d$  can be attributed to the invalidity of the pure adiabatic assumption and coarse spatial resolution of the satellites, it has to be mentioned that the ground-based retrieval strongly relies on the accuracy of the radar reflectivity and therefore also radar calibration and attenuation corrections that are made within the Cloudnet algorithm. Löhnert et al. (2003) points out the strong influence of drizzle on the cloud reflectivity. Errors of 30–60 % have to be anticipated for  $q_L$  profile retrievals. Those retrieval approaches are based on very similar principles as our OE1 method (Löhnert et al., 2001).

## 5 Summary and conclusions

To investigate the accuracy of satellite-based estimates of aerosol indirect effects, we have studied the validity of the adiabatic cloud model as a conceptual tool commonly applied in previous studies (e.g. Bennartz, 2007; Schueller et al., 2003). The adiabatic model allows indirectly to estimate  $H_{\text{cloud}}$  and  $N_d$  from passive satellite observations.

As reference, we used a combination of ground-based active and passive remote sensing instruments with high temporal resolution to provide detailed information of the cloud vertical structure. We could, however, demonstrate that such retrievals also have large uncertainties.

Considering the number of difficulties for both perspectives and those originating from the contrast of two perspectives, our comparison showed that the temporal evolution of cloud micro- and macrophysical quantities is captured surprisingly well for some cases. We discussed the large uncertainties that may occur depending on the observed scene and observation geometry.

The cloud geometrical depth can be obtained with ground-based remote sensing directly from ceilometer cloud base and radar cloud top heights, and by applying the adiabatic method using liquid water path observed with a microwave radiometer. The mean difference of SEVIRI and ground-based adiabatic cloud geometrical depth is lowest for the two homogeneous cases with values down to 49 m (15 %). The overall larger cloud geometrical depth observed with ground-based ceilometer and radar in contrast to the virtual adiabatic one can be explained by subadiabaticity of the cloud layers. The adiabatic factor varied temporally and attained values similar to those reported by Boers et al. (2006). For thin clouds the uncertainties remain large due to the high relative uncertainties of liquid water path and cloud geometrical depth. This also leads to superadiabatic artefacts in the retrieval. With increasing geometrical depth, the clouds become less adiabatic. We also found that clouds are slightly more adiabatic when the cloud profile is dominated by positive Doppler velocity (updrafts). Although a larger dataset would be desirable to draw more robust conclusions in this direction, our re-

Title Page

Abstract

Introduction

Conclusions

References

Tables

Figures



Back

Close

Full Screen / Esc

Printer-friendly Version

Interactive Discussion



sults support those from Schmidt et al. (2014a) and Schmidt et al. (2014b). In general it is desirable to account for subadiabaticity in satellite retrievals.

We developed two similar Optimal Estimation (OE) retrievals to estimate  $N_d$  from ground-based radar and microwave radiometer observations. The main difference is found in the degrees of freedom of the liquid water content profile (adiabatic versus nonadiabatic). This results in differences of  $N_d$ . We found that applying an adiabatic OE approach from ground leads to larger deviations with increasing  $N_d$ . Differences are reflected in the cost function of the adiabatic OE method. Therefore we receive information about which of the retrieved  $N_d$  values deviate from the adiabatic model under the assumption that  $N_d$  is constant vertically.

While the mean difference of  $N_d$  retrieved from SEVIRI and the ground-based nonadiabatic OE was  $78 \text{ cm}^{-3}$  (27 %) for one of the two homogeneous cases, for the second one we saw a large bias of  $367 \text{ cm}^{-3}$  (116 %), whereby the MODIS retrieval was closer to the ground-retrieved one. We were able to attribute this large bias mainly to an underestimation of the effective radius within the current SEVIRI retrieval. Further research about the influence of observation geometry and spatial resolution effects on effective radius and optical depth is required.

The OE approach to retrieve cloud droplet number concentration from ground could be further improved by including more independent observations, e.g. from solar radiation observations (e.g. Brückner et al., 2014).

Indications have been found throughout this study that adjustments to cloud subadiabaticity may help to reduce differences between satellite and ground-based retrievals. For applying such adjustments over larger areas it might be useful to develop a parameterisation of the adiabatic factor depending on cloud geometrical depth. A combination of satellite-derived cloud top height with cloud base height observations from a ground-based ceilometer network would be very interesting. A comparison for cloud geometrical depth using SEVIRI cloud top height and ceilometer cloud base height was already successfully applied by Meerkötter and Bugliaro (2009) for one ground site. Using data from a greater network should be able to gain statistically more robust insights.

Cloud properties from satellite and ground

D. Merk et al.

Title Page

Abstract Introduction

Conclusions References

Tables Figures

◀ ▶

◀ ▶

Back Close

Full Screen / Esc

Printer-friendly Version

Interactive Discussion



Discussion Paper | Discussion Paper | Discussion Paper | Discussion Paper | Discussion Paper

*Acknowledgements.* The first author's work was funded by the Leibzig Graduate School on Radiation (LGS-CAR). We would like to thank the Cloudnet project (European Union Contract EVK2-2000-00611) for providing the ground-based cloud products, and the EUMETSAT SAFS for providing the SEVIRI cloud products, as well as the NASA's Earth-Sun System Division for providing MODIS cloud products. We further acknowledge colleagues participating in the HOPE campaign of the HD(CP)<sup>2</sup> project in Jülich. We also thank our colleagues Anja Hünerbein, Andreas Macke, Fabian Senf and Johannes Quaas for their helpful suggestions and comments.

## References

- Ackerman, A. S., Toon, O. B., Taylor, J. P., Johnson, D. W., Hobbs, P. V., and Ferek, R. J.: Effects of aerosols on cloud albedo: evaluation of Twomey's parameterization of cloud susceptibility using measurements of ship tracks, *J. Atmos. Sci.*, 57, 2684–2695, doi:10.1175/1520-0469(2000)057<2684:EOAOCA>2.0.CO;2, 2000. 5131
- Albrecht, B. A., Fairall, C. W., Thomson, D. W., White, A. B., Snider, J. B., and Schubert, W. H.: Surface-based remote sensing of the observed and the adiabatic liquid water content of stratocumulus clouds, *Geophys. Res. Lett.*, 17, 89–92, doi:10.1029/GL017i001p00089, 1990. 5137
- Bennartz, R.: Global assessment of marine boundary layer cloud droplet number concentration from satellite, *J. Geophys. Res.-Atmos.*, 112, D02201, doi:10.1029/2006JD007547, 2007. 5132, 5141, 5154
- Boers, R., Russchenberg, H., Erkelens, J., Venema, V., van Lammeren, A., Apituley, A., and Jongen, S.: Ground-based remote sensing of stratocumulus properties during CLARA, 1996, *J. Appl. Meteorol.*, 39, 169–181, doi:10.1175/1520-0450(2000)039<0169:GBRSOS>2.0.CO;2, 2000. 5132
- Boers, R., Acarreta, J. R., and Gras, J. L.: Satellite monitoring of the first indirect aerosol effect: retrieval of the droplet concentration of water clouds, *J. Geophys. Res.-Atmos.*, 111, D22208, doi:10.1029/2005JD006838, 2006. 5131, 5138, 5141, 5145, 5154
- Boucher, O., Randall, D., Artaxo, P., Bretherton, C., Feingold, G., Forster, P., Kerminen, V.-M., Kondo, Y., Liao, H., Lohmann, U., Rasch, P., Satheesh, S. K., Sherwood, S., Stevens, B., and Zhang, X. Y.: Clouds and Aerosols, in: *Climate Change 2013: The Physical Science Basis. Contribution of Working Group I to the Fifth Assessment Report of the Intergovernmental*

## Cloud properties from satellite and ground

D. Merk et al.

Title Page

Abstract

Introduction

Conclusions

References

Tables

Figures



Back

Close

Full Screen / Esc

Printer-friendly Version

Interactive Discussion



**Cloud properties  
from satellite and  
ground**

D. Merk et al.

Title Page

Abstract

Introduction

Conclusions

References

Tables

Figures



Back

Close

Full Screen / Esc

Printer-friendly Version

Interactive Discussion



Panel on Climate Change, edited by: Stocker, T. F., Qin, D., Plattner, G.-K., Tignor, M., Allen, S. K., Boschung, J., Nauels, A., Xia, Y., Bex, V., and Midgley, P. M., Cambridge University Press, Cambridge, United Kingdom and New York, NY, USA, 572–657, 2013. 5131

Brenguier, J.-L., Pawlowska, H., Schüller, L., Preusker, R., Fischer, J., and Fouquart, Y.: Radiative properties of boundary layer clouds: droplet effective radius versus number concentration, *J. Atmos. Sci.*, 57, 803–821, doi:10.1175/1520-0469(2000)057<0803:RPOBLC>2.0.CO;2, 2000. 5131, 5138, 5141

Brückner, M., Pospichal, B., Macke, A., and Wendisch, M.: A new multispectral cloud retrieval method for ship-based solar transmissivity measurements, *J. Geophys. Res.-Atmos.*, 119, 11338–11354, doi:10.1002/2014JD021775, 2014. 5155

Cahalan, R. F., Ridgway, W., Wiscombe, W. J., Bell, T. L., and Snider, J. B.: The albedo of fractal stratocumulus clouds, *J. Atmos. Sci.*, 51, 2434–2455, doi:10.1175/1520-0469(1994)051<2434:TAOFSC>2.0.CO;2, 1994. 5163

Chen, R., Wood, R., Li, Z., Ferraro, R., and Chang, F.-L.: Studying the vertical variation of cloud droplet effective radius using ship and space-borne remote sensing data, *J. Geophys. Res.-Atmos.*, 113, D00A02, doi:10.1029/2007JD009596, 2008. 5150

Deneke, H., Knap, W., and Simmer, C.: Multiresolution analysis of the temporal variance and correlation of transmittance and reflectance of an atmospheric column, *J. Geophys. Res.*, 114, D17206, doi:10.1029/2008JD011680, 2009. 5149

Derrien, M.: Algorithm theoretical basis document for cloud products (cma-pge01 v3.2, ct-pge02 v2.2, ctth-pge03 v2.2), Tech. rep., SAFNWC, available at: [http://www.nwcsaf.org/HTMLContributions/SUM/SAF-NWC-CDOP2-MFL-SCI-ATBD-01\\_v3.2.1.pdf](http://www.nwcsaf.org/HTMLContributions/SUM/SAF-NWC-CDOP2-MFL-SCI-ATBD-01_v3.2.1.pdf) (last access: 20 February 2015), 2012. 5134

Dong, X. and Mace, G. G.: Profiles of low-level stratus cloud microphysics deduced from ground-based measurements, *J. Atmos. Ocean. Tech.*, 20, 42–53, doi:10.1175/1520-0426(2003)020<0042:POLLSC>2.0.CO;2, 2003. 5132

Dong, X., Ackerman, T. P., Clothiaux, E. E., Pilewskie, P., and Han, Y.: Microphysical and radiative properties of boundary layer stratiform clouds deduced from ground-based measurements, *J. Geophys. Res.-Atmos.*, 102, 23829–23843, doi:10.1029/97JD02119, 1997. 5132

Dong, X., Mace, G. G., Minnis, P., Smith, W. L., Poellot, M., Marchand, R. T., and Rapp, A. D.: Comparison of stratus cloud properties deduced from surface, GOES, and aircraft data during the march 2000 ARM cloud IOP, *J. Atmos. Sci.*, 59, 3265–3284, doi:10.1175/1520-0469(2002)059<3265:COSECPD>2.0.CO;2, 2002. 5132

**Cloud properties  
from satellite and  
ground**

D. Merk et al.

Title Page

Abstract

Introduction

Conclusions

References

Tables

Figures



Back

Close

Full Screen / Esc

Printer-friendly Version

Interactive Discussion



- Feingold, G., Eberhard, W. L., Veron, D. E., and Previdi, M.: First measurements of the Twomey indirect effect using ground-based remote sensors, *Geophys. Res. Lett.*, 30, 1287, doi:10.1029/2002GL016633, 2003. 5132
- 5 Fox, N. I. and Illingworth, A. J.: The retrieval of stratocumulus cloud properties by ground-based cloud radar, *J. Appl. Meteorol.*, 36, 485–492, doi:10.1175/1520-0450(1997)036<0485:TROSCP>2.0.CO;2, 1997. 5141, 5147
- Frisch, A. S., Feingold, G., Fairall, C. W., Uttal, T., and Snider, J. B.: On cloud radar and microwave radiometer measurements of stratus cloud liquid water profiles, *J. Geophys. Res.-Atmos.*, 103, 23195–23197, doi:10.1029/98JD01827, 1998. 5132
- 10 Han, Q., Rossow, W. B., Chou, J., and Welch, R. M.: Global variation of column droplet concentration in low-level clouds, *Geophys. Res. Lett.*, 25, 1419–1422, doi:10.1029/98GL01095, 1998. 5131
- Hansen, J. E. and Travis, L. D.: Light scattering in planetary atmospheres, *Space Sci. Rev.*, 16, 527–610, 1974. 5138
- 15 Hewison, T.: 1D-VAR retrieval of temperature and humidity profiles from a ground-based microwave radiometer, *IEEE T. Geosci. Remote*, 45, 2163–2168, doi:10.1109/TGRS.2007.898091, 2007. 5143
- Hünerbein, A., Deneke, H., Macke, A., Ebell, K., and Görsdorf, U.: Combining the perspective of satellite- and ground-based observations to analyze cloud frontal systems, *J. Appl. Meteorol. Clim.*, 53, 2538–2552, doi:10.1175/JAMC-D-13-0274.1, 2014. 5131
- 20 Illingworth, A. J., Hogan, R. J., O'Connor, E. J., Bouniol, D., Delanoë, J., Pelon, J., Protat, A., Brooks, M. E., Gaussiat, N., Wilson, D. R., Donovan, D. P., Klein Baltink, H., van Zadelhoff, G.-J., Eastment, J. D., Goddard, J. W. F., Wrench, C. L., Haefelin, M., Krasnov, O. A., Russchenberg, H. W. J., Piriou, J.-M., Vinit, F., Seifert, A., Tompkins, A. M., and Willén U.: Cloudnet: continuous evaluation of cloud profiles in seven operational models using ground-based observations, *B. Am. Meteorol. Soc.*, 88, 883–898, 2007. 5132, 5133, 5135
- 25 Janssen, R. H. H., Ganzeveld, L. N., Kabat, P., Kulmala, M., Nieminen, T., and Roebeling, R. A.: Estimating seasonal variations in cloud droplet number concentration over the boreal forest from satellite observations, *Atmos. Chem. Phys.*, 11, 7701–7713, doi:10.5194/acp-11-7701-2011, 2011. 5139, 5141, 5152
- 30 King, N. J., Bower, K. N., Crosier, J., and Crawford, I.: Evaluating MODIS cloud retrievals with in situ observations from VOCALS-REx, *Atmos. Chem. Phys.*, 13, 191–209, doi:10.5194/acp-13-191-2013, 2013. 5152

**Cloud properties  
from satellite and  
ground**

D. Merk et al.

Title Page

Abstract

Introduction

Conclusions

References

Tables

Figures



Back

Close

Full Screen / Esc

Printer-friendly Version

Interactive Discussion



- Lehmann, K., Siebert, H., and Shaw, R. A.: Homogeneous and inhomogeneous mixing in cumulus clouds: dependence on local turbulence structure, *J. Atmos. Sci.*, 66, 3641–3659, doi:10.1175/2009JAS3012.1, 2009. 5138, 5141
- Löhnert, U., Crewell, S., Simmer, C., and Macke, A.: Profiling cloud liquid water by combining active and passive microwave measurements with cloud model statistics, *J. Atmos. Ocean. Tech.*, 18, 1354–1366, doi:10.1175/1520-0426(2001)018<1354:PCLWBC>2.0.CO;2, 2001. 5132, 5153
- Löhnert, U., Feingold, G., Uttal, T., Frisch, A. S., and Shupe, M. D.: Analysis of two independent methods for retrieving liquid water profiles in spring and summer Arctic boundary clouds, *J. Geophys. Res.-Atmos.*, 108, 4219, doi:10.1029/2002JD002861, 2003. 5153
- Martucci, G. and O'Dowd, C. D.: Ground-based retrieval of continental and marine warm cloud microphysics, *Atmos. Meas. Tech.*, 4, 2749–2765, doi:10.5194/amt-4-2749-2011, 2011. 5132, 5141
- Martucci, G., Milroy, C., and O'Dowd, C. D.: Detection of cloud-base height using Jenoptik CHM15K and Vaisala CL31 ceilometers, *J. Atmos. Ocean. Tech.*, 27, 305–318, doi:10.1175/2009JTECHA1326.1, 2010. 5132, 5139
- Meerkötter, R. and Bugliaro, L.: Diurnal evolution of cloud base heights in convective cloud fields from MSG/SEVIRI data, *Atmos. Chem. Phys.*, 9, 1767–1778, doi:10.5194/acp-9-1767-2009, 2009. 5155
- Meirink, J. F., Roebeling, R. A., and Stammes, P.: Inter-calibration of polar imager solar channels using SEVIRI, *Atmos. Meas. Tech.*, 6, 2495–2508, doi:10.5194/amt-6-2495-2013, 2013. 5135
- Miles, N. L., Verlinde, J., and Clothiaux, E. E.: Cloud droplet size distributions in low-level stratiform clouds, *J. Atmos. Sci.*, 57, 295–311, doi:10.1175/1520-0469(2000)057<0295:CDSIL>2.0.CO;2, 2000. 5143
- Nakajima, T. and King, M. D.: Determination of the optical thickness and effective particle radius of clouds from reflected solar radiation measurements. Part I: Theory, *J. Atmos. Sci.*, 47, 1878–1893, doi:10.1175/1520-0469(1990)047<1878:DOTOTA>2.0.CO;2, 1990. 5134, 5139
- Placidi, S., Roebeling, R., Donovan, D., Boers, R., and Russchenberg, H.: Evaluation of Meteosat-8/SEVIRI retrieved cloud depth for water clouds using CloudNet sites, in: Joint 2007 EUMETSAT Meteorological Satellite Conference and the 15th Satellite Meteorology and Oceanography Conference of the American Meteorological Society, vol. P.50, EUMETSAT, Amsterdam, the Netherlands, 24–28 September 2007, s8–s12, 2007. 5132

## Cloud properties from satellite and ground

D. Merk et al.

Title Page

Abstract

Introduction

Conclusions

References

Tables

Figures



Back

Close

Full Screen / Esc

Printer-friendly Version

Interactive Discussion



- Platnick, S.: Vertical photon transport in cloud remote sensing problems, *J. Geophys. Res.-Atmos.*, 105, 22919–22935, doi:10.1029/2000JD900333, 2000. 5152
- Platnick, S., King, M. D., Ackerman, S. A., Menzel, W. P., Baum, B. A., Riédi, J. C., and Frey, R. A.: The MODIS cloud products: algorithms and examples from Terra, *IEEE T. Geosci. Remote*, 41, 459–473, 2003. 5135
- Quaas, J., Boucher, O., and Lohmann, U.: Constraining the total aerosol indirect effect in the LMDZ and ECHAM4 GCMs using MODIS satellite data, *Atmos. Chem. Phys.*, 6, 947–955, doi:10.5194/acp-6-947-2006, 2006. 5139, 5152
- Rémillard, J., Kollias, P., and Szyrmer, W.: Radar-radiometer retrievals of cloud number concentration and dispersion parameter in nondrizzling marine stratocumulus, *Atmos. Meas. Tech.*, 6, 1817–1828, doi:10.5194/amt-6-1817-2013, 2013. 5132, 5140, 5141
- Rodgers, C.: *Inverse Methods for Atmospheric Sounding – Theory and Practice*, Series on Atmospheric Oceanic and Planetary Physics, World Scientific Publishing Co. Pte. Ltd., edited by: Rodgers, C. D., vol. 2, ISBN:9789812813718, 2000. 5142
- Roebeling, R. A., Feijt, A. J., and Stammes, P.: Cloud property retrievals for climate monitoring: implications of differences between Spinning Enhanced Visible and Infrared Imager (SEVIRI) on METEOSAT-8 and Advanced Very High Resolution Radiometer (AVHRR) on NOAA-17, *J. Geophys. Res.-Atmos.*, 111, D20210, doi:10.1029/2005JD006990, 2006. 5134, 5151
- Roebeling, R., Placidi, S., Donovan, D., Russchenberg, H., and Feijt, A.: Validation of liquid cloud property retrievals from SEVIRI using ground-based observations, *Geophys. Res. Lett.*, 35, L05814, doi:10.1029/2007GL032115, 2008a. 5131, 5144, 5149
- Roebeling, R. A., Deneke, H. M., and Feijt, A. J.: Validation of cloud liquid water path retrievals from SEVIRI using one year of CloudNET observations, *J. Appl. Meteorol. Clim.*, 47, 206–222, doi:10.1175/2007JAMC1661.1, 2008b. 5131
- Rosenfeld, D., Wang, H., and Rasch, P. J.: The roles of cloud drop effective radius and LWP in determining rain properties in marine stratocumulus, *Geophys. Res. Lett.*, 39, L13801, doi:10.1029/2012GL052028, 2012. 5150
- Saunders, R., Matricardi, M., and Brunel, P.: An improved fast radiative transfer model for assimilation of satellite radiance observations, *Q. J. Roy. Meteor. Soc.*, 125, 1407–1425, doi:10.1002/qj.1999.49712555615, 1999. 5134
- Schmetz, J., Pili, P., Tjemkes, S., Just, D., Kerkmann, J., Rota, S., and Ratier, A.: An introduction to Meteosat Second Generation (MSG), *B. Am. Meteorol. Soc.*, 83, 977–992, 2002. 5134

## Cloud properties from satellite and ground

D. Merk et al.

Title Page

Abstract

Introduction

Conclusions

References

Tables

Figures



Back

Close

Full Screen / Esc

Printer-friendly Version

Interactive Discussion



- Schmidt, J., Wandinger, U., and Malinka, A.: Dual-field-of-view Raman lidar measurements for the retrieval of cloud microphysical properties, *Appl. Optics*, 52, 2235–2247, doi:10.1364/AO.52.002235, 2013. 5132
- Schmidt, J., Ansmann, A., Bühl, J., Baars, H., Wandinger, U., Müller, D., and Malinka, A. V.: Dual-FOV Raman and Doppler lidar studies of aerosol-cloud interactions: simultaneous profiling of aerosols, warm-cloud properties, and vertical wind, *J. Geophys. Res.-Atmos.*, 119, 5512–5527, doi:10.1002/2013JD020424, 2014a. 5133, 5146, 5155
- Schmidt, J., Ansmann, A., Bühl, J., and Wandinger, U.: Role of updrafts in aerosol-cloud interactions: lidar observations of layered warm clouds over central Europe, *Atmos. Chem. Phys. Discuss.*, 14, 31409–31440, doi:10.5194/acpd-14-31409-2014, 2014b. 5133, 5155
- Schueller, L., Brenguier, J.-L., and Pawlowska, H.: Retrieval of microphysical, geometrical, and radiative properties of marine stratocumulus from remote sensing, *J. Geophys. Res.*, 108, 8631, doi:10.1029/2002JD002680, 2003. 5131, 5154
- Schulz, J., Albert, P., Behr, H.-D., Caprion, D., Deneke, H., Dewitte, S., Dürr, B., Fuchs, P., Gratzki, A., Hechler, P., Hollmann, R., Johnston, S., Karlsson, K.-G., Manninen, T., Müller, R., Reuter, M., Riihelä, A., Roebeling, R., Selbach, N., Tetzlaff, A., Thomas, W., Werscheck, M., Wolters, E., and Zelenka, A.: Operational climate monitoring from space: the EUMETSAT Satellite Application Facility on Climate Monitoring (CM-SAF), *Atmos. Chem. Phys.*, 9, 1687–1709, doi:10.5194/acp-9-1687-2009, 2009. 5134
- Shupe, M. D.: A ground-based multisensor cloud phase classifier, *Geophys. Res. Lett.*, 34, L22809, doi:10.1029/2007GL031008, 2007. 5132
- Stephens, G. L., Vane, D. G., Boain, R. J., Mace, G. G., Sassen, K., Wang, Z., Illingworth, A. J., O'Connor, E. J., Rossow, W. B., Durden, S. L., Miller, S. D., Austin, R. T., Benedetti, A., Mitrescu, C., and CloudSat Science Team, T.: The CLOUDSAT mission and the A-train, *B. Am. Meteorol. Soc.*, 83, 1771–1790, doi:10.1175/BAMS-83-12-1771, 2002. 5131
- Turner, D. D., Vogelmann, A. M., Johnson, K., Miller, M., Austin, R. T., Barnard, J. C., Flynn, C., Long, C., McFarlane, S. A., Cady-Pereira, K., Clough, S. A., Chiu, J. C., Khaiyer, M. M., Liljegren, J., Lin, B., Minnis, P., Marshak, A., Matrosov, S. Y., Min, Q., O'Hirok, W., Wang, Z., and Wiscombe, W.: Thin liquid water clouds: their importance and our challenge, *B. Am. Meteorol. Soc.*, 88, 177–190, doi:10.1175/BAMS-88-2-177, 2007. 5133
- Twomey, S.: Pollution and the planetary albedo, *Atmos. Environ.*, 8, 1251–1256, doi:10.1016/0004-6981(74)90004-3, 1974. 5130



## Cloud properties from satellite and ground

D. Merk et al.

**Table 1.** Cases used within this study ordered by date. The minimum cloud base height (CBHL) and the maximum cloud top height (CTHL) of the liquid cloud layer investigated are presented together with the temporal averaged inhomogeneity parameter ( $\chi$ ) as in Cahalan et al. (1994) calculated from optical depth of the  $\pm 15$  surrounding SEVIRI pixels for each observation time. Furthermore the category for each case is listed.

Date	Time	Location	Min(CBHL) [m]	Max(CTHL) [m]	$\chi$	category
27 Oct 2011	09:00–13:00 UTC	Leipzig	525 m	1056 m	0.87	homogeneous
1 Jun 2012	12:00–16:00 UTC	Leipzig	1336 m	2428 m	0.73	inhomogeneous
27 Sep 2012	08:00–18:00 UTC	Leipzig	775 m	2927 m	0.55	inhomogeneous
21 Apr 2013	08:00–12:00 UTC	Juelich	1485 m	2171 m	0.87	homogeneous

[Title Page](#)
[Abstract](#)
[Introduction](#)
[Conclusions](#)
[References](#)
[Tables](#)
[Figures](#)

[Back](#)
[Close](#)
[Full Screen / Esc](#)
[Printer-friendly Version](#)
[Interactive Discussion](#)




## Cloud properties from satellite and ground

D. Merk et al.

**Table 3.** Median and SD of the adiabatic factor for all cases and each case individually. Furthermore the median of the adiabatic factor, classified in updraft ( $\nu > 0$ ) and downdraft ( $\nu < 0$ ), and the fraction of subadiabatic cloud profiles is shown. Adiabatic factors with  $f_{\text{ad}} > 1.5$  are omitted since we believe that those are likely affected by measurement uncertainties.

	all	21 Apr 2013	27 Sep 2012	27 Oct 2011	1 Jun 2012
median $f_{\text{ad}}$	0.66	0.64	0.72	0.69	0.47
SD $f_{\text{ad}}$	0.27	0.19	0.32	0.17	0.31
median $f_{\text{ad}} [\nu \geq 0]$	0.69	0.73	0.74	0.72	0.50
SD $f_{\text{ad}} [\nu \geq 0]$	0.27	0.18	0.31	0.16	0.32
median $f_{\text{ad}} [\nu \leq 0]$	0.64	0.62	0.69	0.66	0.44
SD $f_{\text{ad}} [\nu \leq 0]$	0.27	0.18	0.32	0.17	0.70
fraction $f_{\text{ad}} < 1$	0.84	0.99	0.70	0.97	0.85

Title Page

Abstract

Introduction

Conclusions

References

Tables

Figures



Back

Close

Full Screen / Esc

Printer-friendly Version

Interactive Discussion



Cloud properties  
from satellite and  
ground

D. Merk et al.

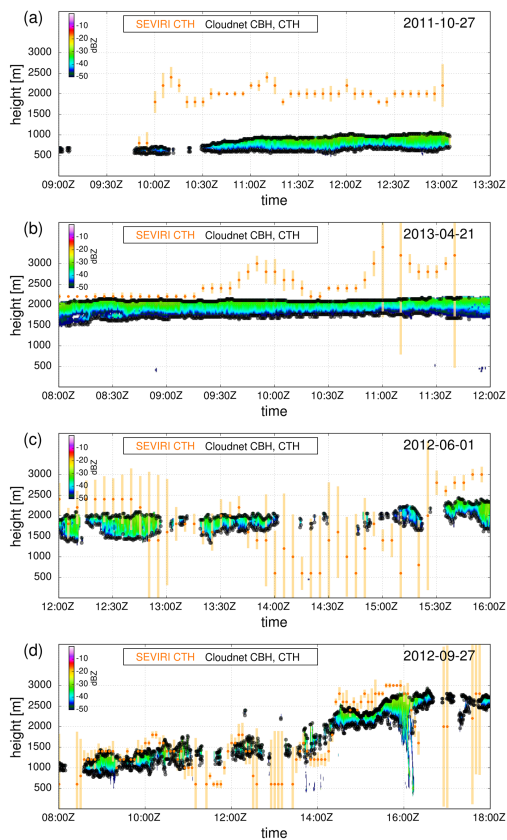


**Figure 1.** Radar reflectivity (in [dBZ]) and cloud borders for the 4 cases listed in Table 1; **(a)** 27 October 2011, **(b)** 21 April 2013, **(c)** 1 June 2012, **(d)** 27 September 2012. Cloud borders are shown as detected by Cloudnet with black dots and by SEVIRI using NWCSAF in orange dots.

[Title Page](#)[Abstract](#)[Introduction](#)[Conclusions](#)[References](#)[Tables](#)[Figures](#)[Back](#)[Close](#)[Full Screen / Esc](#)[Printer-friendly Version](#)[Interactive Discussion](#)

## Cloud properties from satellite and ground

D. Merk et al.

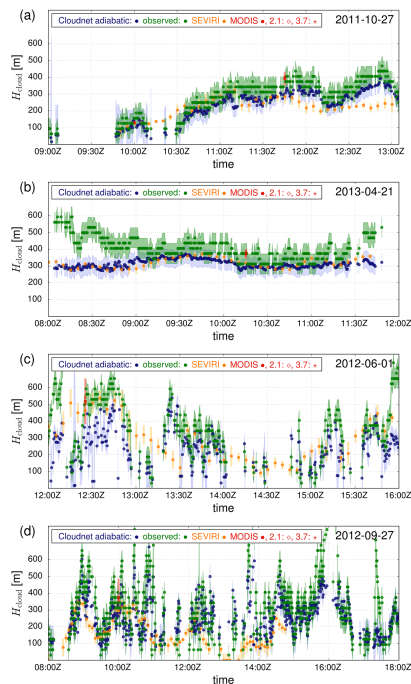


**Figure 2.** Cloud geometrical depth for **(a)** 27 October 2011, **(b)** 21 April 2013, **(c)** 1 June 2012, **(d)** 27 September 2012. Dark blue dots represent the ground-based adiabatic scaled values ( $H_{ad}^{ground}$ ), green dots the ground-observed values ( $H_{obs}^{ground}$ ), yellow dots the SEVIRI adiabatically derived values ( $H_{ad}^{SEVIRI}$ ), and red dots the MODIS adiabatically derived values ( $H_{ad}^{MODIS}$ ). Red diamonds and stars represent the MODIS adiabatically derived values using available channels 2.1 and 3.7  $\mu\text{m}$ , respectively. The uncertainty for the ground-based values is shown as shaded areas in the same color type as the dots. Variability for SEVIRI and MODIS is given in terms of SD of the surrounding area of  $\pm 1$  and  $\pm 9$  pixels, respectively.

[Title Page](#)
[Abstract](#)
[Introduction](#)
[Conclusions](#)
[References](#)
[Tables](#)
[Figures](#)

[Back](#)
[Close](#)
[Full Screen / Esc](#)
[Printer-friendly Version](#)
[Interactive Discussion](#)


Cloud properties  
from satellite and  
ground

D. Merk et al.

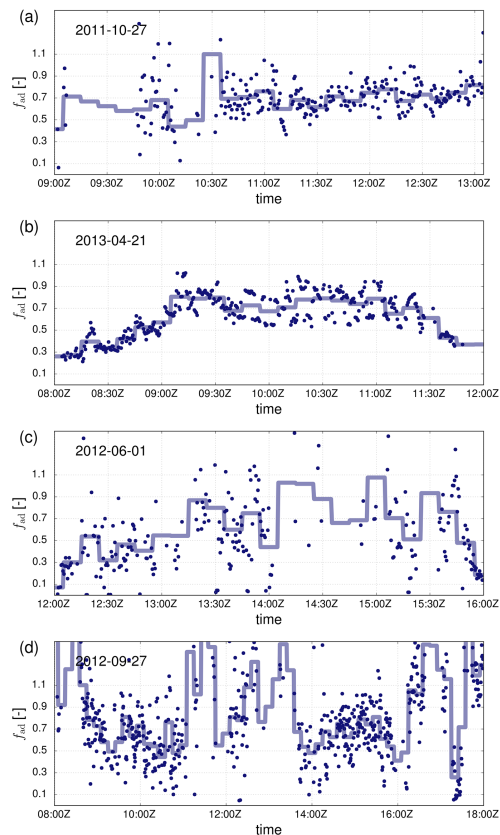


**Figure 3.** Adiabatic factor for **(a)** 27 October 2011, **(b)** 21 April 2013, **(c)** 1 June 2012, **(d)** 27 September 2012. Blue dots represent the adiabatic factor derived using  $H_{obs}^{ground}$  and  $Q_L$  from the microwave radiometer. The blue line represents the interpolated and 10 min averaged values.

[Title Page](#)[Abstract](#)[Introduction](#)[Conclusions](#)[References](#)[Tables](#)[Figures](#)[Back](#)[Close](#)[Full Screen / Esc](#)[Printer-friendly Version](#)[Interactive Discussion](#)

## Cloud properties from satellite and ground

D. Merk et al.

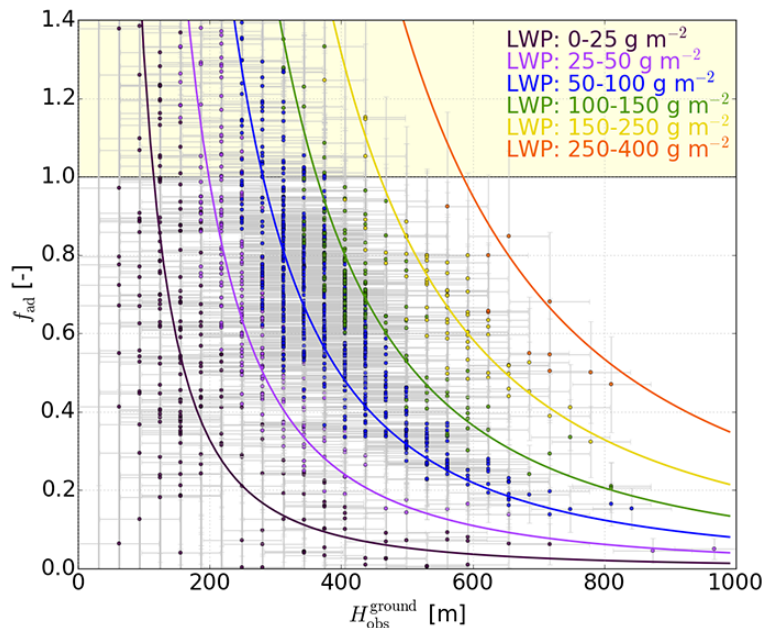


**Figure 4.** Adiabatic factor as a function of observed cloud geometrical depth ( $H_{\text{obs}}^{\text{ground}}$ ) including data of all 4 cases. Colors indicate different liquid water path bins. The range with  $f_{\text{ad}} > 1$  is shaded with light yellow. The solid lines represent the relationship described in Eq. (8) for bin mean liquid water path and  $\Gamma_{\text{ad}} = 1.9 \times 10^{-3} \text{ g m}^{-4}$ .

Title Page

Abstract

Introduction

Conclusions

References

Tables

Figures



Back

Close

Full Screen / Esc

Printer-friendly Version

Interactive Discussion



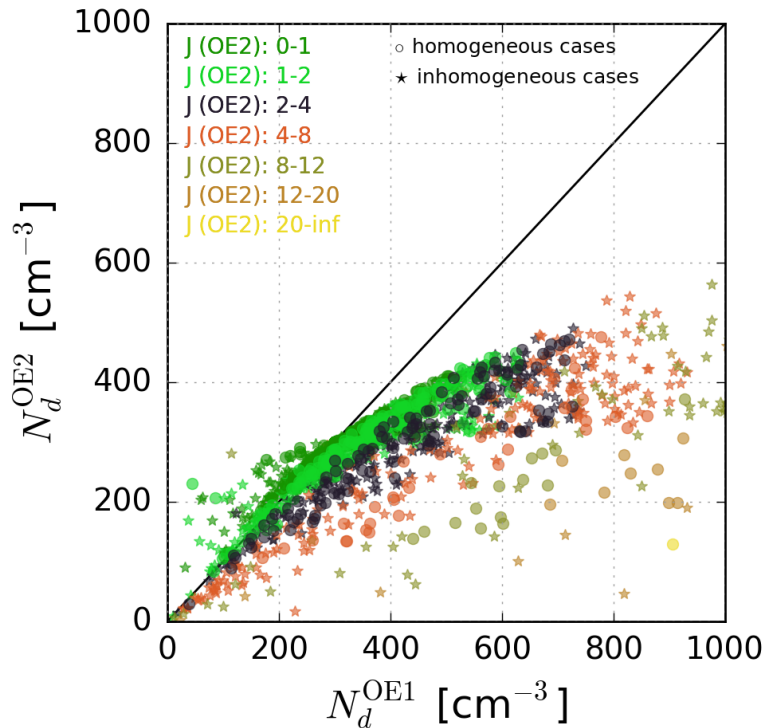


**Figure 5.** Comparison of the retrievals of cloud droplet number concentration using OE1 and OE2 method. The color represents the remaining cost function of the OE2 method after the optimization. The black line represents the 1 : 1 relationship.

Cloud properties from satellite and ground

D. Merk et al.

Title Page	
Abstract	Introduction
Conclusions	References
Tables	Figures
◀	▶
◀	▶
Back	Close
Full Screen / Esc	
Printer-friendly Version	
Interactive Discussion	



## Cloud properties from satellite and ground

D. Merk et al.

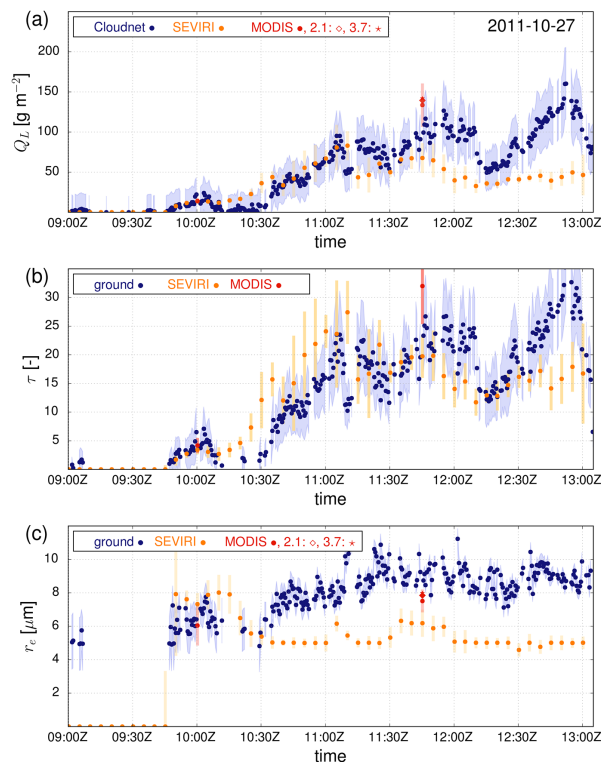


**Figure 6.** (a) Liquid water path for 27 October 2012 as obtained from the microwave radiometer (dark blue dots), adiabatically from SEVIRI (yellow dots) and MODIS (red). For MODIS the effective radius obtained with three different channels is shown with different symbols (diamond: 2.1  $\mu\text{m}$ , dot: 1.6  $\mu\text{m}$ , star: 3.7  $\mu\text{m}$ ). The uncertainty estimates are represented in the same way as described in Fig. 2. (b) Time series of optical depth as obtained from SEVIRI (yellow), MODIS (red), and calculated from ground retrievals (blue). (c) Time series of effective radius with the same colors.

## Cloud properties from satellite and ground

D. Merk et al.

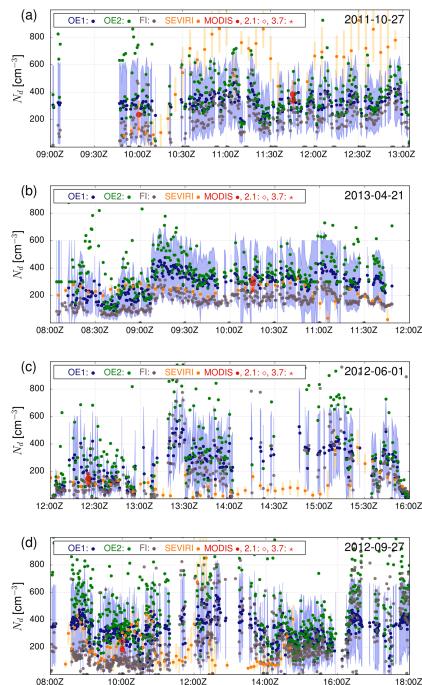


**Figure 7.** Time series of retrievals of the estimated cloud droplet number concentration. Blue dots represent the OE1 method, using ground-based data ( $N_d^{OE1}$ ). The blue shaded area represents the uncertainty, calculated from the error covariance matrix of OE1. Green dots represent the OE2 method ( $N_d^{OE2}$ ). Gray dots represent the retrieval with the FI method applied to ground site data ( $N_d^{FI}$ ). Orange dots represent the adiabatically derived values from SEVIRI ( $N_d^{SEVIRI}$ ), while red dots those from MODIS ( $N_d^{MODIS}$ ). Different MODIS channels used in the retrieval are denoted with the same symbols as in the figures before. Variability for SEVIRI and MODIS is given in terms of SD of the surrounding area of  $\pm 1$  and  $\pm 9$  pixels, respectively.

[Title Page](#)
[Abstract](#)
[Introduction](#)
[Conclusions](#)
[References](#)
[Tables](#)
[Figures](#)

[Back](#)
[Close](#)
[Full Screen / Esc](#)
[Printer-friendly Version](#)
[Interactive Discussion](#)


## Cloud properties from satellite and ground

D. Merk et al.

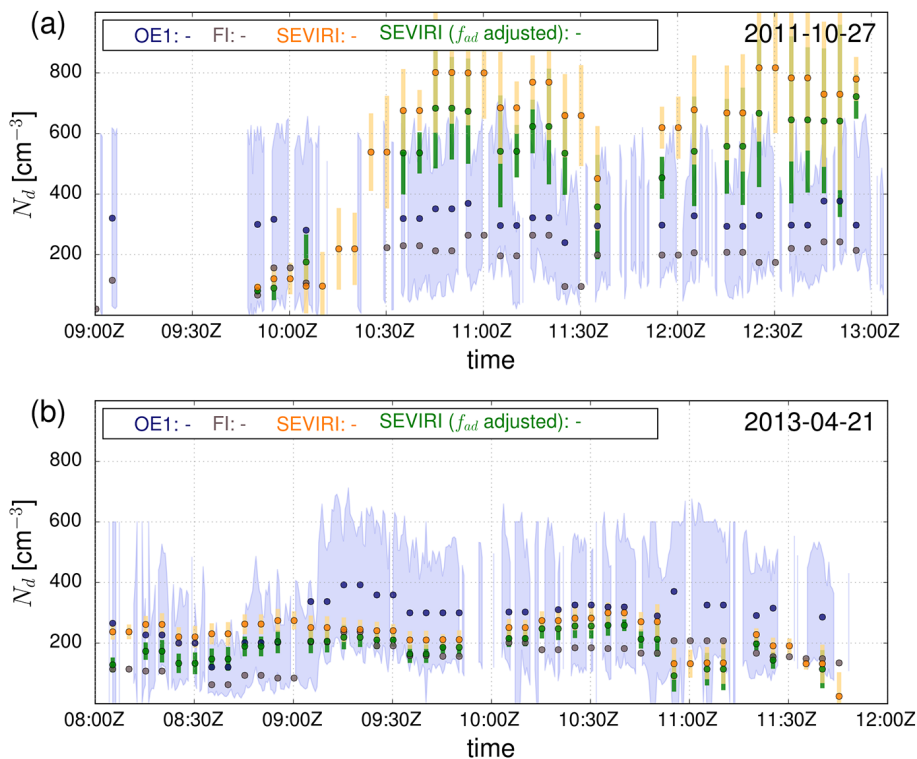


**Figure 8.** 10 min averaged  $N_d$  for the two homogeneous cases. As Fig. 7, but with additional  $N_d^{\text{SEVIRI}}$  adjusted by the adiabatic factor (green dots).

Title Page

Abstract

Introduction

Conclusions

References

Tables

Figures

◀

▶

◀

▶

Back

Close

Full Screen / Esc

Printer-friendly Version

Interactive Discussion

